Analysis of Coating Thickness Variation During Optical Fiber Processing

Qibo Jiang, Fuzheng Yang, and Ranga Pitchumani

***Abstract*—During the mass production of silica-based optical fibers, a large fiber preform is softened in a high-temperature furnace and is drawn to a small fiber with a diameter of about 125 μm. The hot fiber exiting the furnace is cooled rapidly by the surrounding air or by blowing a gas, and is subsequently coated with a polymer layer to provide a protection of the fiber surface. The overall quality of the fiber depends on the uniformity of the coating layer, which is strongly influenced by the manufacturing conditions. While the average thickness of the coating layer is extensively investigated in the literature, the studies on the coating thickness fluctuation lack a sound fundamental basis. In this paper, a linear perturbation analysis is adopted to predict the coating thickness variation under different processing conditions. An experimental correlation is developed to determine the initial amplitude of the thickness disturbance. Numerical results are presented for the first time to directly link the processing and geometric parameters with the coating thickness fluctuation in the final product. The results provide guidelines for selecting coating materials, system designs, and processing parameters to achieve uniform fiber coating layers.**

***Index Terms*—Coating thickness fluctuation, optical fiber coating, perturbation analysis.**

NOMENCLATURE

a	Dimensionless fiber radius R_f/h_0 defined in (10).
A_i	Initial amplitude.
A_f	Final amplitude.
B	Coefficients in (13).
Ca	capillary number $= \mu V_f/\sigma$.
Ca_0	reference capillary number $= \mu W_0/\sigma$ in (10).
d	complex wave celerity $= d_r + id_i$.
d_i	Amplitude growth rate.
d_{id}	Dimensional amplitude growth rate [s^{-1}].
Fr	Froude number $= V_f^2/gR_f$.
g	Gravitational acceleration [m^2/s].
h	Local coating thickness [m].
h_0	Average coating thickness [m].
L	Length of the coating die [m].
Oh	Ohnesorge number $= \mu/\sqrt{\rho\sigma R_f}$.
p_{in}	Pressure at the applicator inlet [Pa].
p_a	Atmosphere pressure [Pa].
R_f	Fiber radius [m].
R_d	Inner radius of the applicator die [m].
Re	Reynolds number $= \rho V_f R_f/\mu$.
Re_0	reference Reynolds number $= \rho W_0 h_0/\mu$ in (10).
$Re_{\max}$	Maximum Reynolds number for an acceptable final amplitude.
r	Radial coordinate [m].
S	dimensionless group $= [Oh Ca/\sqrt{Fr}]^2$.
t	Time [s].
V_f	Drawing velocity [m/s].
W_0	Maximum velocity for the fully developed flow [m/s].
z	Axial coordinate for an inertial reference frame with velocity V_f [m].
Z	Dimensionless axial coordinate for a reference frame at rest.

Greek symbols

α	$2\pi h_0/\lambda$ wavenumber defined in (10).
α_m	Critical wavenumber.
η	Dimensionless coating thickness variation.
λ	Surface wave length [m].
μ	Dynamic viscosity [Ns/m^2].
ψ	Stream function [m^3/s].
ρ	Density [kg/m^3].
σ	Surface tension [N/m].

Manuscript received June 24, 2004; revised November 30, 2004. This work was supported in part by the National Science Foundation Information Technology Research program under Grant CTS-0112822.

The authors are with the Advanced Materials amd Technologies Laboratory, Department of Mechanical Engineering, University of Connecticut, Storrs, CT 06269 USA (e-mail: r.pitchumani@uconn.edu).

Digital Object Identifier 10.1109/JLT.2005.843519

I. INTRODUCTION

FABRICATION of optical fibers has achieved impressive advances to meet the tremendous demand from various communication applications. However, the technology is still based largely on empirical approaches with a relatively lagging use of scientific understanding of the inherent thermal-fluid transport processes that are responsible for the optical and mechanical properties of the fiber. A fiber production system may be divided into three major functional regions: 1) heating; 2) cooling; and 3) coating regions [1]. In the heating region, a large silica-based preform (>8 cm in diameter) is softened in a graphite or zirconia furnace with temperatures between 1400 °C to 2300 °C. The preform is drawn into small fiber with 125 μm nominal diameter, forming a neck-down geometry. To meet the mass production requirement, it is desirable to adopt high drawing speeds. Drawing tension in the heating (or neck-down) region must be controlled to be small since large tension may cause strength degradation of the final product [1]. The high strength of glass fibers is primarily due to the flawless conditions of their surfaces, which are susceptible to external damage [1]–[3]. Thus, a protective coating layer is applied on the fiber surface by passing the fiber through a coating applicator in the coating region. The coating materials are mostly polymers

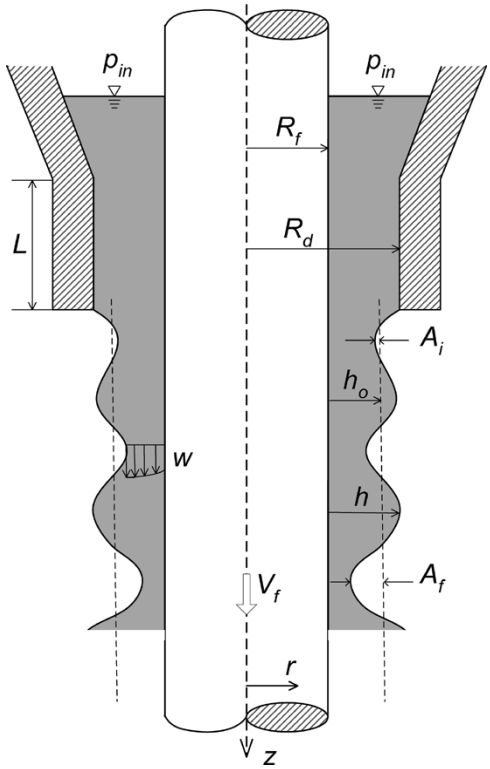

Fig. 1. Schematic of the optical fiber coating process.

such as acrylate that may degrade with temperature $T > 80\,^{\circ}\mathrm{C}$, therefore, a cooling region consisting of forced and/or natural convective cooling is usually present before the applicator to reduce the fiber temperature as it enters the coating region with lower temperature.

A schematic of the optical fiber coating region is shown in Fig. 1, where a fiber with radius R_f is drawn through an applicator filled with coating liquid at a velocity V_f in the z-direction. The applicator has a conical segment at the top and followed by a cylindrical segment (called coating die) with a length L and an inner radius R_d. A pressure p_{in} is imposed at the inlet of the applicator, and a free surface with varying coating thickness h, along the fiber axis z, is formed after the coating die exit. The coated fiber is passed through an ultraviolet radiation region (outside the range of Fig. 1) to cure the liquid polymer, forming the solid coating layer on the fiber surface.

Extensive studies on the transport phenomena in the heating and cooling zones have been conducted, and a comprehensive review is given by Paek [1]. In the coating zone, the average coating thickness and its fluctuation are important issues, and severe variation of the coating thickness may cause transportation losses of optical signal and weaken the mechanical properties of the fiber [4]. The average coating thickness was determined in the literature by a simple analysis of the flow within the coating die with the following assumptions: 1) fully developed flow in the cylindrical die; 2) constant properties; 3) negligible surface tension and viscous heating [5]–[7]. Assumption 1 is justified by the fact that typical coating flow is laminar with Reynolds number $Re < 1$, and the entrance length L_e (proportional to Re) required for the flow development is much smaller than the die length L. Note that internal heating by viscous dissipation may be significant for coating fluids with high viscosity and at high drawing rates. Moreover, the viscosity may vary within the coating die owing to the nonuniform temperature in the region. Analysis of the process including the effects of viscous heating and temperature-dependent rheology may be conducted in a future work by solving the energy equation coupled with the momentum equation for the flow. Further, the analyzes presented here assume perfect alignment of the fiber axis with that of the cylindrical die, and no vibration of the fiber during the manufacturing process. The average coating thickness h_0 was obtained as a function of the pressure difference between the applicator and the die exit Δp, drawing velocity V_f, coating material viscosity μ, and geometric parameters R_f, R_d, and L [5]–[7].

$$\frac{h_0}{R_2} = \left[\frac{\Delta p R_d^2}{8\mu L V_f}\left(1 - k^4 + \frac{(1-k^2)^2}{\ln k}\right) - \frac{1-k^2}{2\ln k}\right]^{\frac{1}{2}} - k \tag{1}$$

where $k = R_f/R_d$.

To the knowledge of the authors, the thickness fluctuation of the coating layer in the coating region has been the subject of little attention due to the complex dynamics of the free surface. The thickness fluctuation of the coating layer is governed by the internal flow in the applicator and the external flow with a free surface between the die exit and the inlet of the cure oven. With the increase of the drawing velocity, experimental studies show that the thickness fluctuation of the coating layer may increase dramatically, and may lead to the formation of discrete beads on the fiber surface [5], [8], [9]. The shear stress of the coating flow at the die exit is also found to be responsible for the thickness fluctuation [4]. Other manufacturing conditions, such as pressure, coating material properties, and applicator die geometry may also influence the uniformity of the coating thickness.

The external flow down a vertical cylinder (i.e., fiber) may be extremely unstable, causing significant variation of coating thickness. Perturbation analyzes on a film flow down a cylindrical substrate are commonly seen in the literature (for example, [10]–[17]). Lin and Liu [11] solved the stability problem of the free coating of moving wires and tubes, and the necessary condition for the stability of the film coating was given in terms of the Reynolds number Re, a wavenumber α, the drawing velocity V_f, and a Weber number We which may be related to the reference capillary number Ca_0, defined later in this paper. Goren [12] found that the critical wavelength α_c corresponding to the most rapid growth of fluctuation amplitude was a function of the fiber-coating die radius ratio k, and the reciprocal of the square of the Ohnesorge number Oh. Lin and Weng [13] employed the linear stability theory to study the characteristics of condensate film flow down a vertical cylinder, and the effects of the surface tension and the mass transfer due to phase change at the liquid-vapor interface were addressed. The curvature of cylinder was reported to intensify the instability of the flow in comparison with the planar flow. Cheng *et al.* [16] investigated the weakly nonlinear stability characteristic of a viscoelastic film flowing down a vertical cylinder. Both the viscoelastic effect and the curvature of the cylinder were found to enhance the flow instability.

During the optical fiber coating process, the amplitude of the thickness fluctuation increases from an initial value A_i at the die

exit (Fig. 1) to a final value A_f (Fig. 1) at the inlet to the ultraviolet curing zone with an exponential growth rate d_i. The goal of the present paper is to predict the final thickness variation as a function of the processing and geometrical parameters. Since the aforementioned stability theories can only predict the amplitude growth rate, experimental data were used in this study to developed a correlation of the initial amplitude, which, in turn, was used to determine A_f. In the next section, the perturbation theory is applied to the coating flow after the die exit, and an experimental correlation for A_i is derived in Section III. Based on the instability analysis and the correlations, a systematic study is conducted to elicit the effects of different processing and geometrical parameters on the coating thickness fluctuation.

II. Instability Analysis

Consider the coating flow of an incompressible Newtonian fluid on the fiber surface after the die exit, as shown in Fig. 1. With respect to a reference frame moving with the constant drawing velocity V_f, the governing equations for the axisymmetric flow in cylindrical coordinates may be written as

$$\frac{\partial u}{\partial r}+\frac{u}{r}+\frac{\partial w}{\partial z}=0 \tag{2}$$

$$\rho\left(\frac{\partial u}{\partial t}+u\frac{\partial u}{\partial r}+w\frac{\partial u}{\partial z}\right)=-\frac{\partial p}{\partial r}+\mu\left[\frac{\partial}{\partial r}\left(\frac{1}{r}\frac{\partial (ur)}{\partial r}\right)+\frac{\partial^2 u}{\partial z^2}\right] \tag{3}$$

$$\rho\left(\frac{\partial w}{\partial t}+u\frac{\partial w}{\partial r}+w\frac{\partial w}{\partial z}\right)=-\frac{\partial p}{\partial z}+\mu\left[\frac{1}{r}\frac{\partial}{\partial r}\left(r\frac{\partial w}{\partial r}\right)+\frac{\partial^2 w}{\partial z^2}\right]+\rho g \tag{4}$$

where u and w are the velocity components in the r and z directions, respectively, p is the pressure, ρ is the density, g is the constant of gravity acceleration, and μ is the viscosity.

The boundary conditions corresponding to the above governing equations are: 1) no-slip conditions at the fiber surface; 2) the vanishing of shear stress on the free surface; 3) the balance of normal stress on the free surface; and 4) the kinematic condition. The mathematical expressions for these conditions may be written as [16]

$$w(z,R_f)=0;\quad u(z,R_f)=0 \tag{5}$$

$$\left(\frac{\partial w}{\partial r}+\frac{\partial u}{\partial z}\right)+2\left(\frac{\partial w}{\partial z}-\frac{\partial u}{\partial r}\right)\times\frac{\partial h}{\partial z}\left[\left(\frac{\partial h}{\partial z}\right)^2-1\right]^{-1}=0 \tag{6}$$

$$p-p_a-\sigma\left(\frac{1}{r\left[1+\left(\frac{\partial h}{\partial z}\right)^2\right]^{\frac{1}{2}}}-\frac{\frac{\partial^2 h}{\partial z^2}}{\left[1+\left(\frac{\partial h}{\partial z}\right)^2\right]^{\frac{3}{2}}}\right)=2\mu\left[\frac{\partial u}{\partial r}-\left(\frac{\partial w}{\partial r}+\frac{\partial u}{\partial z}\right)\frac{\partial h}{\partial z}+\frac{\partial w}{\partial z}\left(\frac{\partial h}{\partial z}\right)^2\right]\times\left[1+\left(\frac{\partial h}{\partial z}\right)^2\right]^{-1} \tag{7}$$

$$u=\frac{\partial h}{\partial t}+w\frac{\partial h}{\partial z} \tag{8}$$

where σ is the surface tension, p_a is the atmosphere pressure, t is the time, h is the local coating thickness, and the velocity components are expressed in terms of a stream function ψ as

$$u=\frac{1}{r}\frac{\partial \psi}{\partial z}\quad w=-\frac{1}{r}\frac{\partial \psi}{\partial r}. \tag{9}$$

It must be pointed out that the vanishing of shear stress at the free surface may need to be further verified at high drawing velocities, since the air flow in the vicinity of the coating surface may cause a finite drag on the coating surface. This will be considered in a future extension of the analysis.

A set of dimensionless quantities may be defined as [16]

$$\begin{aligned}
&p^*=\frac{p-p_a}{\rho W_0^2};\quad \alpha=\frac{2\pi h_0}{\lambda};\quad z^*=\frac{\alpha z}{h_0}\\
&r^*=\frac{r}{h_0};\quad t^*=\frac{\alpha W_0 t}{h_0};\quad Ca_0=\frac{\mu W_0}{\sigma}\\
&\psi^*=\frac{\psi}{W_0 h_0^2};\quad a=\frac{R_f}{h_0};\quad h^*=\frac{h}{h_0}\\
&q=a+h^*;\quad Re_0=\frac{\rho W_0 h_0}{\mu};\quad \sigma^*=\left(\frac{\sigma^3\rho}{4\mu^4 g}\right)^{\frac{1}{3}}
\end{aligned} \tag{10}$$

where h_0 is the average coating thickness, λ is the surface wave length, and W_0 is the maximum velocity in the z direction for the stable and fully developed flow at the downstream, and is driven by the gravity [16]

$$W_0=\frac{\rho g h_0^2}{4\mu\gamma} \tag{11}$$

in which $\gamma=[2(1+a)^2 log((1+a)/a)-(1+2a)]^{-1}$. Other symbols in (10) are defined in the nomenclature. The dimensionless governing equations and boundary conditions may be readily obtained from (4)–(10) and are omitted here for brevity. It must be mentioned that the dimensionless group σ^* is obtained from the boundary condition in the normal direction of the free surface [i.e., (7)] where the gravity, viscous, and surface tension forces contribute to the force balance. Note that the gravity may be an important driving force for the coating flow when the drawing velocity is small, but may be relatively insignificant for high speed drawing.

Since small wavenumber α [defined in (10)] is typically observed in the phenomenon of film instability, the solution of the dimensionless stream function ψ^* and pressure p^* may be expanded as power series of α [16]

$$\begin{aligned}
\psi^*&=\psi_0^*+\alpha\psi_1^*+0(\alpha^2)\\
p^*&=p_0^*+\alpha p_1^*+0(\alpha^2).
\end{aligned} \tag{12}$$

Following the steps in perturbation analysis [16], (12) is substituted into (4)–(8) to obtain systems of ordinary differential equations for the first two orders of α, which, in turn, are solved analytically. Substituting the solutions of ψ^* and p^* into the kinematic condition (8) a generalized linear kinematic equation is obtained as

$$\frac{\partial h^*}{\partial t}+B_1(h^*)\frac{\partial h^*}{\partial z^*}+B_2(h^*)\frac{\partial^2 h^*}{\partial z^{*2}}+B_3\frac{\partial^4 h^*}{\partial z^{*4}}=0 \tag{13}$$

where $B_1(h^*)$, $B_2(h^*)$, and $B_3(h^*)$ are given as

$$\begin{aligned}
B_1 &= 2\gamma\left(q^2-a^2-2q^2\ln\frac{q}{a}\right)\\
B_2 &= -Re_0\alpha\gamma^2C_1-Re_0\alpha\gamma^2C_2q^4a^2-2\alpha\sigma^*Re_0^{-\frac{2}{3}}(2\gamma)^{\frac{1}{3}}\frac{1}{q^3}\\
&\quad\times\left[\frac{3}{16}q^4+\frac{1}{16}a^4-\frac{1}{4}q^2a^2-\frac{1}{4}q^4\ln\frac{q}{a}\right]\\
B_3 &= -2\sigma^*Re_0^{-\frac{2}{3}}(2\gamma)^{\frac{1}{3}}\frac{\alpha^3}{q}\\
&\quad\times\left[\frac{3}{16}q^4+\frac{1}{16}a^4-\frac{1}{4}q^2a^2-\frac{1}{4}q^4\ln\frac{q}{a}\right]\\
C_1 &= \left(\frac{5}{2}\left(\ln\frac{q}{a}\right)^2-\frac{59}{48}-2\left(\frac{q}{a}\right)^3\right)q^6-\frac{13}{48}a^6\\
&\quad+a^4q^2\left(\frac{9}{16}-\frac{7}{4}\ln\frac{q}{a}\right)\\
C_2 &= -\frac{1}{2}(\ln a)^2+\frac{1}{2}(\ln q)^2-\frac{1}{2}\ln q-\ln a\times\ln\frac{q}{a}\\
&\quad+\frac{1}{2}\ln a+\frac{19}{4}\ln\frac{q}{a}+\frac{15}{16}-3\left(\ln\frac{q}{a}\right)^2.
\end{aligned}\tag{14}$$

Defining a dimensionless coating thickness variation η as $\eta(t^*,z^*)=h^*(t,z^*)-1$, the evolution of thickness variation η is obtained from (13) as

$$\frac{\partial\eta}{\partial t^*}+B_1\frac{\partial\eta}{\partial z^*}+B_2\frac{\partial^2\eta}{\partial z^{*2}}+B_3\frac{\partial^4\eta}{\partial z^{*4}}=0 \tag{15}$$

where the values of B_1, B_2, and B_3 are evaluated at the dimensionless average coating thickness $h^*=1$.

Recall that the discussion so far is based on a moving reference frame with speed V_f. To obtain the evolution of thickness fluctuation for a coordinate system at rest, the following Gallilean transformation is [11] applied to (15)

$$Z=z^*+\frac{V_f}{W_0}t^* \tag{16}$$

and the resulting thickness fluctuation equation may be written as

$$\frac{\partial\eta}{\partial t}+\left(B_1-\frac{V_f}{W_0}\right)\frac{\partial\eta}{\partial Z}+B_2\frac{\partial^2\eta}{\partial Z^2}+B_3\frac{\partial^4\eta}{\partial Z^4}=0. \tag{17}$$

A general solution of (17) is expressed in the following form

$$\eta=A_i\exp\left(\frac{d_iZW_0}{V_f}\right)\cos(Z-d_rt^*) \tag{18}$$

where A_i is the initial perturbation amplitude, the dimensionless linear wave speed d_r, and the exponential growth rate of the amplitude (dimensionless) d_i are given as

$$d_r=B_1-\frac{V_f}{W_0};\quad d_i=B_2-B_3. \tag{19}$$

The case of $B_1=V_f/W_0$ corresponds to a static wave with speed $d_r=0$, for which (18) indicates that the wave shape does not change with time. Note that the initial amplitude A_i appears as an undetermined coefficient in the solution of η, and needs to be determined from additional considerations described in the next section. Equation (18) indicates that the coating thickness varies as a cosine wave along the fiber axial direction, and the amplitude of the wave grows exponentially with time. The amplitude of the thickness variation in the final product A_f is evaluated from (18), at a location Z_f as

$$A_f=A_i\exp\left(\frac{d_iZ_fW_0}{V_f}\right) \tag{20}$$

where Z_f is the dimensionless distance from the coating die exit to the entrance of the cure region. Equation (20) indicates that the final amplitude of an unstable flow (i.e., with $d_i>0$) increases with the increase in Z_f. Values of d_i being greater than zero, therefore, signify an unstable coating process.

III. Correlation of the Initial Amplitude

The coating flow from the applicator inlet to the die exit is responsible for the value of the initial amplitude A_i involved in the perturbation analysis. A scaling analysis of the governing equations and the boundary conditions of the flow reveals the following dimensionless groups: 1) Reynolds number $Re=\rho V_fR_f/\mu$; 2) dimensionless inlet pressure ratio $p_{\rm in}/p_a$; 3) dimensionless group $S=[OhCa/\sqrt{Fr}]^2$; 4) aspect ratio L/R_f; and 5) radius ratio R_d/R_f. Note that the geometry of the conical segment of the applicator is ignored since it has negligible effect on the fully developed flow in the coating die. Evidently, the initial amplitude is a function of the aforementioned dimensionless groups. The initial amplitude is also governed by disturbances such as the moving fiber and environmental effects. However, theoretical analysis of A_i is not available in the literature, owing to poorly understood mechanisms that initiate the fluctuation of the free surface flow. To facilitate the prediction of thickness fluctuation in the optical fiber coating process, a readily usable empirical correlation is developed in this section, and is assumed to have a general form

$$\begin{aligned}
A_i &= C_1\left(\frac{R_d}{R_f}\right)^{n_1}\left(\frac{L}{R_f}\right)^{n_2}\left(\frac{p_{\rm in}}{p_a}\right)^{n_3}S^{n_4}\\
&\quad\times\exp(S^{n_5}Re^{n_6})\\
&= f_1\exp(f_2Re^{n_6}).
\end{aligned}\tag{21}$$

The assumption of A_i being proportional to the exponential of Re^{n_6} is based on the experimental observation that the initial amplitude has a superexponential growth rate with increasing Reynolds number (see the data from Wagatsuma *et al.* [8] in Fig. 2). Furthermore, the influence of the parameter S is separated into two parts: one as a power law variation S^{n_4} and the second as an exponential variation, based on this form yielding a closer agreement with available data. Power law variations are assumed for the remaining dimensionless groups in the above correlation. For the current experimental data, (21) gives satisfactory correlation as presented.

Fig. 2 shows the initial amplitude A_i as a function of the Reynolds number Re for various values of the dimensionless group S wherein the symbols are experimental data from Wagatsuma *et al.* [8] and the lines denote correlation results based on (21). The data correspond to the parameter combination of $p_{\rm in}/p_a=1$, $L/R_f=32$, and $R_d/R_f=3.2$. Since only the final amplitude was reported in the original experimental data,

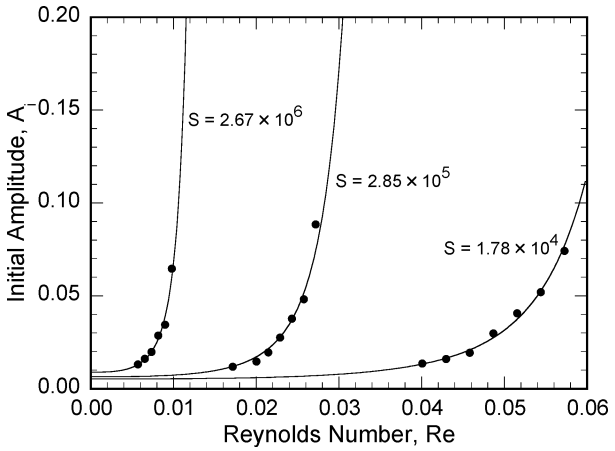

Fig. 2. Variation of the initial amplitude as a function of Reynolds number, Re, and the dimensionless group S. Symbols denote experimental data from Wagatsuma *et al.* [8], and the lines denote best fit correlation through data.

the values of A_i were inferred from A_f using (20). Furthermore, the distance between the coating die exit and inlet of the cure oven is not reported in the literature, and is taken to be 400 times the fiber radius R_f in this paper. The initial amplitude is seen to increase monotonically with increasing Reynolds number or S. A value of $n_6 = 3$ shows the best fit for all the three values of S in Fig. 2, and the corresponding values of f_1 and f_2 [defined in (21)] were obtained for each value of S. Note that A_i has finite values when the disturbance caused by the drawing velocity is zero (i.e., $Re = 0$), owing to additional perturbation sources (e.g., fiber vibration) in the system. The existence of nonzero A_i when $Re = 0$ is also consistent with the results of perturbation analysis in [10]–[17].

The variation of f_1 and f_2 with S is shown in Fig. 3(a) and (b), in which the symbols are the numerical results obtained from Fig. 2, and the solid lines denote linear regression fit through the data on a log-log scale. According to (21), the slopes of the best fit lines in Fig. (3a) and (b) correspond to the constants $n_4 = 0.1023$ and $n_5 = 0.964$, respectively. Fig. 4(a) shows the experimental data from Kobayashi *et al.* [9] on the initial amplitude as a function of the dimensionless inlet pressure ratio p_{in}/p_a. It is observed that A_i decreases monotonically with increasing p_{in}/p_a. Based on the same reasoning as that in Fig. 3(a) and (b), the slope of the linear fit in Fig. 4(a) is used to determine the constant $n_3 = -3.85$.

Since no experimental data is available on the initial amplitude A_i as a function of the geometric parameter R_d/R_f (or L/R_f) alone, while keeping all the other parameters constant, (21) is rearranged as follows to determine the exponent n_1 (or n_2).

$$f_3 = C_1 \left(\frac{R_d}{R_f}\right)^{n_1} = \frac{A_i}{\left[\left(\frac{L}{R_f}\right)^{n_2}\left(\frac{p_{\text{in}}}{p_a}\right)^{n_3} S^{n_4}\exp(S^{n_5}Re^{n_6})\right]}$$
$$f_4 = C_1 \left(\frac{L}{R_f}\right)^{n_2} = \frac{A_i}{\left[\left(\frac{R_d}{R_f}\right)^{n_1}\left(\frac{p_{\text{in}}}{p_a}\right)^{n_3} S^{n_4}\exp(S^{n_5}Re^{n_6})\right]}. \quad (22)$$

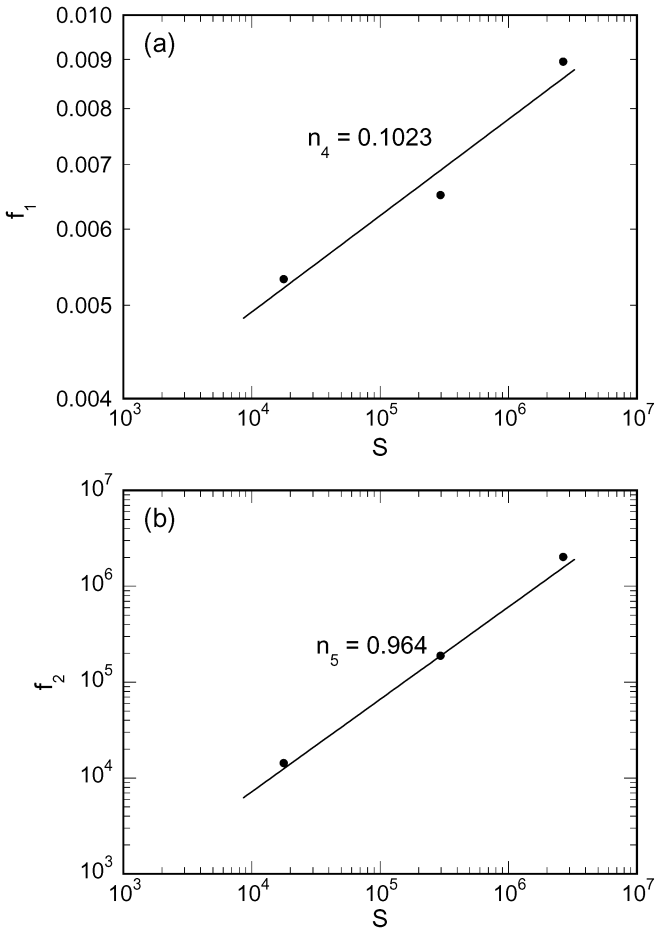

Fig. 3. The functions f_1 and f_2 used to determine the constants n_4 and n_5 in (21).

Fig. 4(b) shows f_3 as a function of the radius ratio R_d/R_f, where the symbols are obtained from experimental data of Panoliaskos *et al.* [5], and a value of $n_1 = -1.5$ is determined from the slope. The values of f_4 obtained from the data of Panoliaskos *et al.* [5] and Wagatsuma *et al.* [8] are presented in Fig. 4(c) for two values of the aspect ratio L/R_f, and n_2 is found to be -0.5 from the slope.

Note that Figs. 2–4 are used to determine the power exponents in (21) through experimental data from three sources, while the proportionality constant C_1 is determined using the experimental data from Panoliaskos *et al.* [5] and Wagatsuma *et al.* [8]. The data of Kobayashi *et al.* [9] could not be used in the determination of C_1 since the values of the parameters S, Re, R_d/R_f, and L/R_f were not reported by the authors. Equation (21) implies that the three values of f_1 in Fig. 3(a) can be used to determine the proportionality constant C_1 via the relation $C_1 = f_1/[(R_d/R_f)^{n_1}(L/R_f)^{n_2}(p_{\text{in}}/p_a)^{n_3}S^{n_4}]$, while (22) indicates that C_1 may be obtained by equating the two y-intercepts in Fig. 4(b) and (c) to $\log C_1$. Thus, five values of C_1 are obtained, and the average value is used in the final expression of the correlation

$$A_i = 0.079\left(\frac{R_d}{R_f}\right)^{-1.5}\left(\frac{L}{R_f}\right)^{-0.5} \times \frac{p_{\text{in}}}{p_a}^{-3.85} S^{0.1023}\exp(S^{0.964}Re^3). \quad (23)$$

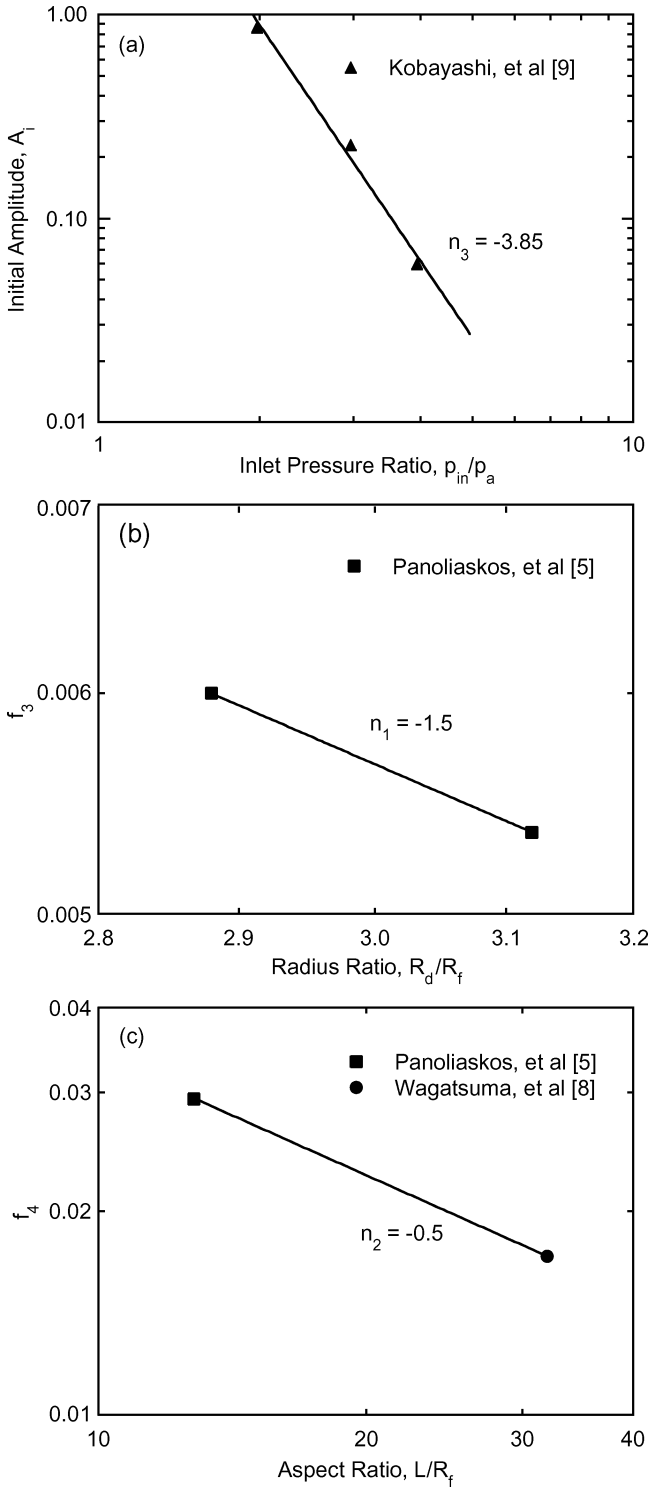

Fig. 4. (a) Experimental data on the initial amplitude as a function of the inlet pressure ratio, $p_{\rm in}/p_a$. (b) f_3 as a function of the radius ratio R_d/R_f. (c) f_4 as a function of the aspect ratio L/R_f.

The asymptotic trends of (23) with respect to the Reynolds number Re and the dimensionless group S are consistent with physical expectation. The initial amplitude increases monotonically with increasing Re and S, owing to the greater disturbance introduced as explained in the next section. When $Re \to 0$, the coating flow is driven by the pressure and the gravity, and A_i is determined by the remaining four dimensionless groups. For the case $S \to 0$, A_i approaches zero since large surface tension stabilizes the coating flow. With the increase in the dimensionless pressure, the friction force at the die exit is relatively small, leading to a smaller perturbation and initial amplitude. Furthermore, A_i increases with decreasing R_d/R_f and L/R_f, owing to thinner coating layer that is susceptible to external disturbance. Equation (23), therefore, captures the dominant physical effects of the process and serves as an appropriate correlation for the current experimental data. The overall comparison between the correlation, (23), and the experimental data is presented in Fig. 5. The diagonal line in the plot corresponds to the line of exact agreement and the dashed lines denote 10% error bands. As seen in the figure, the correlation fits well with experimental data over the range of parameters considered. A total of 35 data points are presented in the plot, most of which are seen to lie within the 10% error bands.

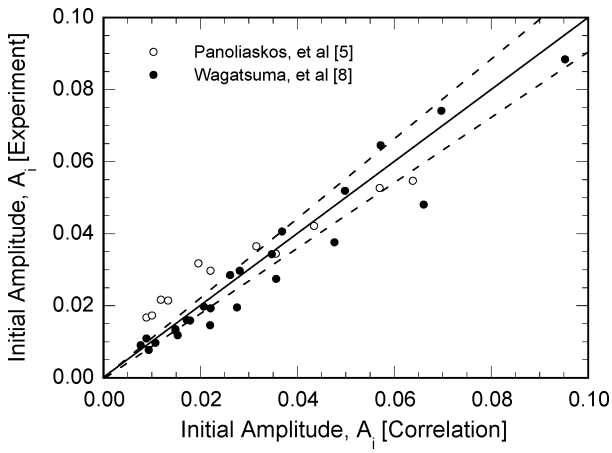

Fig. 5. Summary comparison of the empirical correlation with experimental data on the initial amplitude.

IV. Results and Discussion

The fluctuation of coating thickness obtained from the instability analysis [i.e., (18)] and the correlation of the initial amplitude with available experimental data [(23)] are combined to describe the thickness fluctuation in the optical fiber coating process. In this section, numerical results are presented to illustrate the effects of the processing and applicator geometric parameters on the uniformity of the coating thickness. The amplitude growth rate d_i is first presented as a function of the wavenumber and the Reynolds number, and it is shown that the values of d_i are positive, indicating that the fiber coating process is inherently unstable. The wavenumber corresponding to the maximum growth rate is then presented to identify the frequency at which the worst thickness fluctuation occurs for a given combination of processing conditions. Furthermore, the amplitude of thickness variation in the final product and the thickness variation along the fiber axis are directly linked to the processing and geometrical parameters. The results are aimed at providing guidelines for selecting processing parameters, coating materials, and coater geometries to achieve desired coating thickness and overall optical fiber properties.

Fig. 6 shows the growth rate of the amplitude d_i as a function of the wavenumber α and the Reynolds number Re. The results

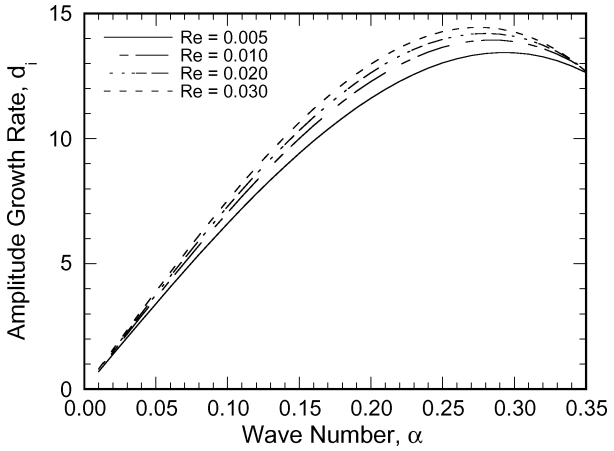

Fig. 6. Amplitude growth rate d_i as a function of the wavenumber, α and the Reynolds number Re. The results correspond to the parameter combination of $S = 10^5$, $p_{\text{in}}/p_a = 1.5$, $R_d/R_f = 3.0$, and $L/R_f = 22.5$.

correspond to the parameter combination of $S = 10^5$, $p_{\text{in}}/p_a = 1.5$, $R_d/R_f = 3.0$, $L/R_f = 22.5$, and the range of Reynolds number is considered to be from 0.005 to 0.05. The values of the parameters are chosen to be representative of typical coating process conditions. For a fixed Reynolds number, the growth rate d_i reaches a maximum with increasing wavenumber α, which may be explained by the resonance phenomenon of a dynamic system, where the amplitude grows rapidly near a critical resonant frequency. The fluctuation of the coating thickness, therefore, attains a maximum at a critical wavenumber α_m. The growth rate increases monotonically with increasing Re, owing to the intensified disturbance from a moving fiber at higher speed.

Overall, the growth rate d_i has limited increase with increasing Reynolds number. Very weak dependence of d_i on Re is observed for both small values $(\alpha < 0.05)$ and large values $(\alpha > 0.30)$ of the wavenumber. When $\alpha = 0.010$ and 0.303, the growth rates are about 0.7 and 13.4, respectively, for all the values of Reynolds number considered in this study. As the value of α approaches the resonant frequencies (around $\alpha = 0.25$), the increase of d_i with increasing Re becomes more apparent. For example, for the case of $\alpha = 0.25$, d_i increases from 13.02 to 14.27 when Re increases from 0.005 to 0.030. The limited dependence of the growth rate d_i on Re is in favor of the requirement of mass production of optical fiber, since the draw velocity may be increased with little adverse influence on the thickness fluctuation. All the values of d_i in Fig. 6 are positive, which correspond to exponential growth of the coating thickness fluctuation with time (or along the fiber axial direction). Consequently, the distance between the coating die exit and the cure oven must be strictly controlled such that the growth of the thickness fluctuation does not exceed a tolerable level.

The frequency of the disturbance, i.e., the wavenumber α, is observed to have significant influence on the growth rate. As α increases from 0.01 to 0.303, d_i increases nearly twenty folds from about 0.7 to about 13.4. The values of d_i near the critical frequencies are excessively large (between 13.0 and 15.0) for all the Reynolds numbers, which indicates that the fiber coating process is extremely unstable in the particular frequency range.

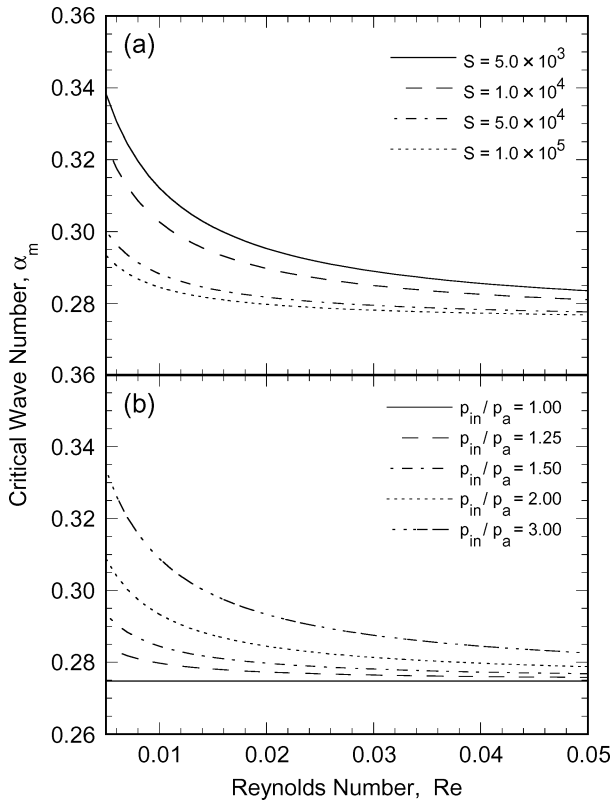

Fig. 7. Critical wavenumber α_m as a function of the Reynolds number Re for different (a) dimensionless group S and (b) inlet pressure ratio p_{in}/p_a. The default values of the parameters are $R_d/R_f = 3.0$, $L/R_f = 22.5$. (a) $p_{\text{in}}/p_a = 1.5$ and (b) $S = 10^5$.

Equation (19) shows that $d_i = B_2 - B_3$, where B_2 is proportional to α, while B_3 is proportional to α^3. Therefore, as α increases further beyond 0.303, it is expected that d_i will decrease monotonically. It must be pointed out that the growth rate d_i may change from positive to negative as α approaches infinity, which corresponds to the transition of the coating process from the unstable to the stable regime [16]. Dimensional results for the growth rate are included in the Appendix for easier understanding of the physical process. In Fig. 6, the critical wavenumber, α_m, at different Reynolds number changes from 0.26 to 0.30, and the effects of the processing and geometric parameters on the α_m are systematically discussed in Figs. 7 and 8.

Fig. 7(a) shows the critical wavenumber α_m as a function of the Reynolds number Re at different values of the dimensionless group S. The results are based on the same parameter combinations as in Fig. 6, except for S and Re. For a fixed value of S, the critical wavenumber decreases monotonically with increasing Reynolds number, which is consistent with the results seen in Fig. 6. The trend may be explained by considering the definition of the wavenumber (10) and the expression for the coating thickness (1). When Reynolds number increases, the coating becomes thinner by virtue of increasing V_f in (1), which, in turn, corresponds to a smaller wavenumber. The increase in the critical wavenumber with decreasing S may be explained as follows. An increase in S may be attributed either to increased viscosity μ or to decreased surface tension σ. For a fixed driving pressure p_{in}/p_a in the coating die, the flow rate decreases with

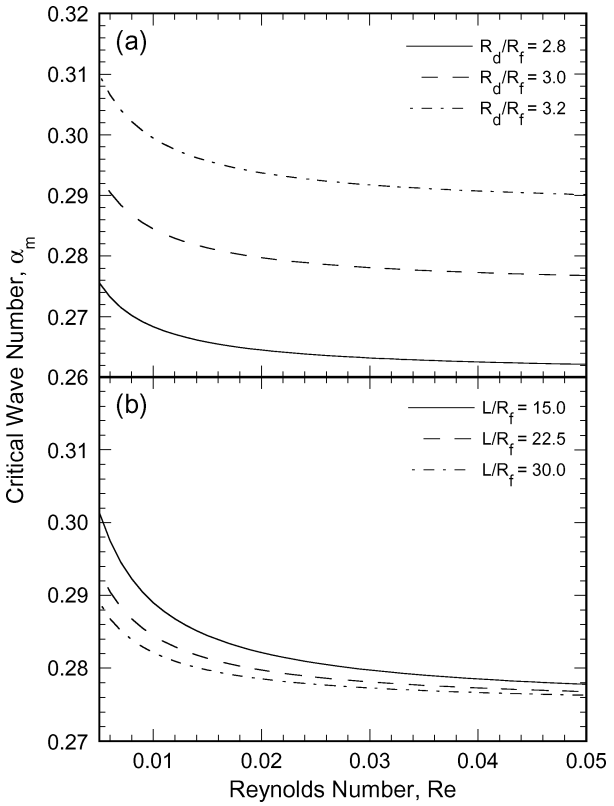

Fig. 8. Critical wavenumber α_m as a function of the Reynolds number Re for different (a) radius ratio R_d/R_f and (b) aspect ratio L/R_f. The default values of the parameters are $p_{\rm in}/p_a = 1.5$, $S = 10^5$. (a) $L/R_f = 22.5$ and (b) $R_d/R_f = 3.0$.

increasing viscosity, and again yields a thinner coating on the fiber, for a given V_f. The surface tension influences the pressure at the die exit p_o via the relation $p_a - p_o = \sigma/R$, where R is the curvature of the meniscus at the die exit, and p_a is the ambient pressure [2]. Evidently, p_o increases with decreasing σ, which leads to a smaller pressure difference and flow rate in the coating die. It follows, therefore, that an increase in S results in a decrease in flow rate and the coating thickness, leading to smaller wavenumber α_m, as seen in Fig. 7(a).

In Fig. 7(b), the influence of the inlet pressure ratio $p_{\rm in}/p_a$ on the the critical wavenumber is demonstrated. The results correspond to $S = 10^5$, with all the other parameters retaining their values in Fig. 7(a). Since an increase in $p_{\rm in}/p_a$ corresponds to increased flow rate and coating thickness, the wavenumber increases monotonically with increasing $p_{\rm in}/p_a$ at fixed Reynolds number. Again, α_m decreases with increasing Re, as previously explained in Fig. 7(a). However, for an open cup coating process, i.e., $p_{\rm in}/p_a = 1.0$, experimental data show that the effect of Reynolds number on the coating thickness is insignificant [5]. Consequently, the critical wavenumber is almost invariant with Re for the case $p_{\rm in}/p_a = 1.0$ in Fig. 7(b). Note that the values of α_m in Fig. 7(a) and (b) lie within the range 0.26–0.33, which is consistent with the findings of Goren [12]. For the range of $R_f/h_0 > 0.25$, the critical wavenumber is found to only weakly dependent on the five dimensionless groups in (23) (i.e., Re, $p_{\rm in}/p_a$, S, L/R_f, and R_d/R_f), and is within the range 0.25–0.35, as shown both from theoretical analysis and experimental measurements by Goren [12]. The nominal coating thickness in Fig. 7(a) and (b) corresponds to $a = 0.5$, and the values of α_m are found to be within the range reported by Goren [12].

The effects of the geometric parameters of the coating die, i.e., the radius ratio R_d/R_f and the aspect ratio L/R_f, on the critical wavenumber α_m are presented in Fig. 8(a) and (b), respectively. Several studies have demonstrated that the coating thickness increases linearly with increasing die diameter for constant fiber diameter [1], [2], [5]. Based on the reasoning in Fig. 7(a) and (b) that larger coating thickness corresponds to a larger wavenumber, α_m is seen to increase monotonically with increasing R_d/R_f in Fig. 8(a). The frictional resistance in the coating die increases with increasing aspect ratio L/R_f, which leads to smaller flow rate and coating thickness. Therefore, the increase of L/R_f has the opposite effect as the increase of R_d/R_f [Fig. 8(b)]. Again, the critical wavenumber decreases monotonically with the Reynolds number and the values of α_m in Fig. 8(a) and (b) are within the range 0.25–0.35 discussed previously. Overall, all the parameters discussed in Figs. 7 and 8 influence the critical wavenumber through the coating thickness, and limited changes in α_m are observed.

The final amplitude of coating thickness variation in the product, i.e., A_f, is of direct interest in the evaluation of the product quality. Recall that the perturbation solution (20) and the correlation of the initial amplitude (23) are used simultaneously to determine A_f. The influence of the processing and geometric parameters on A_f is shown in Figs. 9 and 10. In all the calculations, the critical wavenumber is adopted to give conservative estimation of A_f.

Fig. 9(a) illustrates the influence of the Reynolds number Re and the dimensionless group S on the final amplitude A_f. Since the initial amplitude A_i increases exponentially with increasing Re (see Fig. 2) and the amplitude growth rate d_i also increases with Re (see Fig. 6), the final amplitude A_f increases monotonically with Re for a fixed value of S in Fig. 9(a). The parameter S governs the viscosity and surface tension of the coating material, and has significant influence on the stability of the coating surface. A large value of S corresponds to relatively small surface tension or large viscosity ratio between the coating layer and the air. As pointed out in [18] and [19], both small surface tension and large viscosity ratio are responsible for unstable interface between two fluids. Consequently, the final amplitude is seen to increase monotonically with increasing S for a fixed Reynolds number. When $S = 10^4$, the final amplitude A_f is smaller than 0.005 for the entire range of Reynolds number (0.005–0.05) considered in this study. To keep A_f below 0.005 for the case $S = 5 \times 10^5$, however, the Reynolds number has to be decreased substantially to 0.011. Evidently, a coating material with low viscosity and high surface tension is desirable for maintaining coating thickness uniformity in the fibers. The maximum allowable Reynolds number $Re_{\max}$, denoted in Fig. 9(a) for each combination of the other parameters will be discussed later in this section.

Fig. 9(b) shows the final amplitude as a function of Reynolds number at different inlet pressure ratio $p_{\rm in}/p_a$. Note that the fluid flow in the fiber coating process is driven by two driving forces: (1) the moving fiber (i.e., the fiber speed); and (2) the applicator inlet pressure $p_{\rm in}/p_a$. Due to the movement of the fiber,

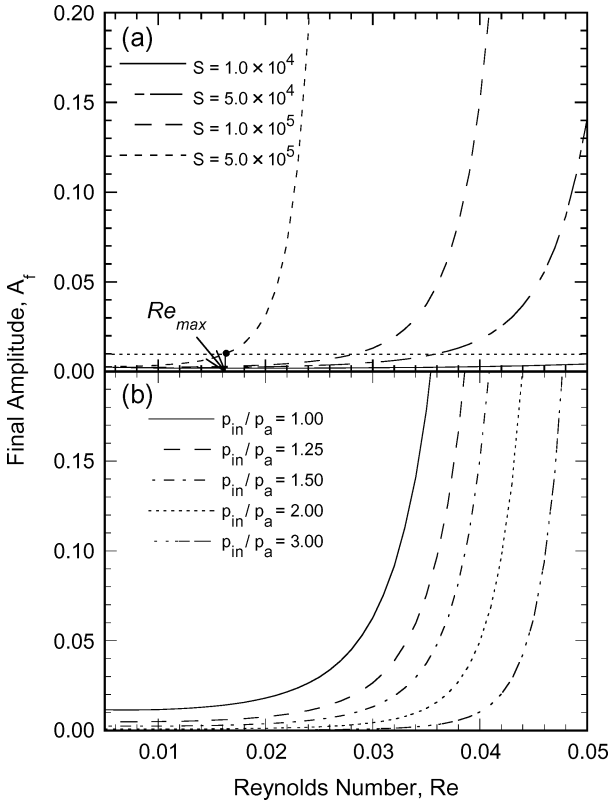

Fig. 9. Final amplitude A_f as a function of the Reynolds number Re for different (a) dimensionless group S. (b) Inlet pressure ratio $p_{\rm in}/p_a$. The default values of the parameters are $R_d/R_f = 3.0$, $L/R_f = 22.5$. (a) $p_{\rm in}/p_a = 1.5$. (b) $S = 10^5$.

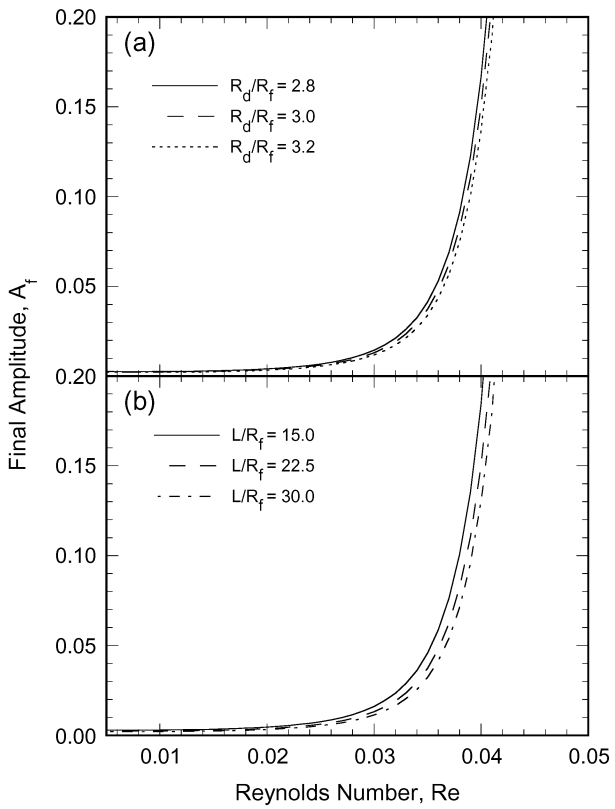

Fig. 10. Final amplitude A_f as a function of the Reynolds number Re for different (a) radius ratio R_d/R_f and (b) aspect ratio L/R_f. The default values of the parameters are $p_{\rm in}/p_a = 1.5$, $S = 10^5$. (a) $L/R_f = 22.5$ and (b) $R_d/R_f = 3.0$.

a large shear stress may develop at the die exit, which is considered to be a major reason for unstable flow causing undesirable coating thickness variation. The use of a pressurized applicator $p_{\rm in}/p_a > 1$ is aimed at minimizing the aforementioned shear stress by synchronizing the speeds of the coating fluid and the fiber. When $p_{\rm in}/p_a$ increases from the open cup case $p_{\rm in}/p_a = 1$ to the pressurized applicator case $p_{\rm in}/p_a = 3$, (23) indicates that the initial amplitude decreases monotonically, resulting in a decrease in the final thickness amplitude A_f. The final amplitude A_f increases exponentially with Re, as previously discussed in Fig. 9(a). It must be pointed out that an extremely large value of applicator pressure may cause the fluid to have higher speed than the fiber in the coating die, which in turn leads to a high shear stress on the fiber. Evidently, therefore, an optimal pressure exists for each value of Reynolds number to obtain zero shear stress at the die exit.

The effects of the geometric parameters R_d/R_f and L/R_f on the final amplitude A_f are presented in Fig. 10(a) and (b), respectively. The range of values of the geometric parameters are chosen to cover typical die designs in the optical fiber manufacturing process. It is observed that the final amplitude A_f decreases with increasing R_d/R_f [Fig. 10(a)] or increasing L/R_f [Fig. 10(b)]. These trends for A_f are consistent with the experimental data for the initial amplitude A_i in Fig. 4(b) and (c), which suggests that A_i decreases monotonically with increasing radius ratio R_d/R_f and aspect ratio L/R_f. Overall, the influence of the geometric parameters on the final amplitude is much less significant than that of the processing parameters shown in Fig. 9(a) and (b).

The results in Figs. 9 and 10 establish the relationship between the final amplitude and the processing and geometric parameters. Furthermore, from a process design viewpoint, it will be useful to derive quantitative ranges of the parameters corresponding to acceptable thickness fluctuation level. To this end, a maximum value of the Reynolds number $Re_{\max}$ is obtained for each combination of the other parameters such that the final amplitude A_f is smaller than a limiting value. If the acceptable variation is limited to 1%, i.e., $A_f = 0.01$, the maximum Reynolds number may be obtained from Figs. 9 and 10 as the intersection of a horizontal line at $A_f = 0.01$ with each of the curve, as illustrated in Fig. 9(a) for the case of $S = 5 \times 10^5$.

Fig. 11(a) presents two processing parameters S and $p_{\rm in}/p_a$ as functions of the maximum Reynolds number $Re_{\max}$ calculated from Fig. 9(a) and (b), respectively. When the dimensionless group S decreases, the free surface tends to be more stable and a higher drawing velocity (or larger $Re_{\max}$) may be adopted for the coating process. For the case of $S = 10^4$, the maximum Reynolds number $Re_{\max}$ is larger than 0.05, which may correspond to larger production rate than that commonly achieved in the optical fiber industry. The dimensionless inlet pressure ratio, $p_{\rm in}/p_a$, is seen to increase with increasing $Re_{\max}$, owing to more stable free surface at higher inlet pressure of the applicator. When $p_{\rm in}/p_a = 1$, the final amplitude is larger than 1% for the entire range of Reynolds number, which indicates that

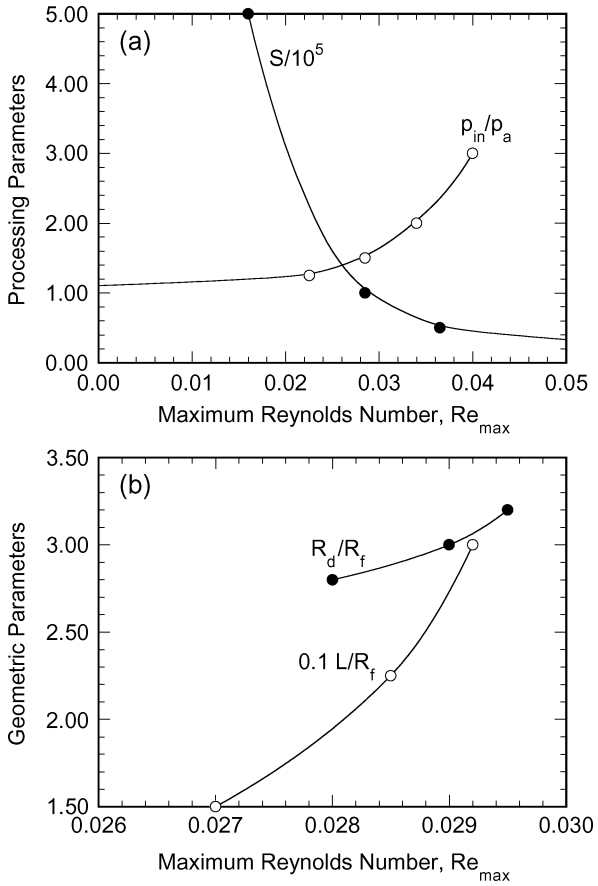

Fig. 11. The processing parameters (a) S and $p_{\rm in}/p_a$, and (b) the geometric parameters R_d/R_f and L/R_f as functions of the maximum Reynolds number $Re_{\rm max}$.

the open cup setup is not appropriate for the parameter combination in Fig. 11(a).

Following the same approach as in Fig. 11(a), the radius ratio R_d/R_f and the aspect ratio L/R_f are obtained as functions of $Re_{\rm max}$ from Fig. 10(a) and (b), respectively, and are shown in Fig. 11(b). Since the coating flow becomes more stable as the values of both ratios increase, larger drawing velocity (or $Re_{\rm max}$) may be used for the coating process with increasing R_d/R_f and L/R_f. However, for the range of the geometric parameters considered in the study, the maximum Reynolds number shows relatively small variation.

Fig. 11(a) and (b) serves as useful design tool for determining the maximum allowable drawing velocity for a given combination of design and processing parameters from the viewpoint of coating thickness uniformity. This information, together with the coating flow model and the correlation presented in this paper, will in turn enable an accurate design of the process parameters for an application. It must be mentioned that physical mechanisms contributing to the initial amplitude A_i are still not well understood. Theoretical and experimental investigations are imperative in a future work to directly determine A_i as a function of the processing conditions. In a possible approach, numerical solution of the flow field from the inlet of the applicator to the inlet of the cure region may be used to determine the free surface location and fluctuation, which in turn, may be used to determine the initial amplitude A_i as a function of the dimensionless groups presented in this paper. Furthermore, the assumptions of isothermal system with negligible viscous heating and shear stress at the free surface must be relaxed in a future work toward more accurate simulation of the coating process at high speeds.

V. Conclusion

An optical fiber coating process is investigated in this paper with the focus on the description of the coating thickness variation as function of the relevant material, processing, and geometric parameters. A linear perturbation analysis is employed to determine the thickness fluctuation η as a function of the initial amplitude A_i, the amplitude growth rate d_i, the wave speed d_r, the axial location Z, and growth time t^*. An empirical correlation is developed based on experimental data available in the literature to relate the initial amplitude to dimensionless processing parameters S, Re, $p_{\rm in}/p_a$, and geometric parameters R_d/R_f and L/R_f. The results of the study revealed that the processing parameters have a more pronounced influence on A_i than the geometric parameters, for the range of parameters considered. The perturbation growth rate d_i increases with the increase in Reynolds number, and a maximum of d_i is achieved at a critical wavenumber α_m. For typical optical fiber manufacturing conditions, the value of α_m is found to vary in a small range from 0.26 to 0.33. The final amplitude of the coating thickness fluctuation, as the fiber enters the curing region, increases with increase in Reynolds number Re and the dimensionless group S, and with decrease in dimensionless inlet pressure ratio $p_{\rm in}/p_a$, aspect ratio L/R_f, and radius ratio R_d/R_f. The maximum Reynolds number, which relates to the maximum drawing velocity, for a given combination of other process parameters was determined so as to limit fluctuation of coating thickness to within an acceptable maximum.

Appendix

Three nondimensional results in the present paper, i.e., Figs. 6, 7(a), and 9(b), are reduced to dimensional form in Fig. 12(a), (b), and (c), respectively, for easier interpretation of the predictions. In Fig. 12(a), the dimensional amplitude growth rate $d_{id} = d_i(\alpha W_0/h_0)$ is presented as a function of the drawing velocity V_f, and the reciprocal of the wave length $1/\lambda$. The results correspond to the parameter combination of viscosity $\mu = 4$ Ns/m^2, density $\rho = 1100$ kg/m^3, surface tension $\sigma = 0.0284$ N/m, inlet pressure $P_{\rm in} = 1.5$ atm, fiber radius $R_f = 62.5$ μm, die radius $R_d = 187.5$ μm, and die length $L = 1.4$ mm. For fixed drawing velocity, the trend in Fig. 12(a) follow those in Fig. 6, namely, d_{id} reaches a peak value with increasing $1/\lambda$. With increasing drawing velocity, both the coating thickness h_0 and the velocity W_0 [see (11)] decrease, leading to the reduced d_{id} in Fig. 12(a). Note that d_{id} holds small positive values for the range of parameter combinations considered, and the maximum value of d_{id} in Fig. 12(a) is seen to be 3.9×10^{-5} s^{-1} when $V_f = 0.3$ m/s and $1/\lambda = 944$ m^{-1}. Since the distance between the coater and the cure oven is taken to be 0.1 m in this paper, the physical time for the coating thickness fluctuation development changes from 0.333 s to 0.056 s when V_f increases from 0.3 to 1.8

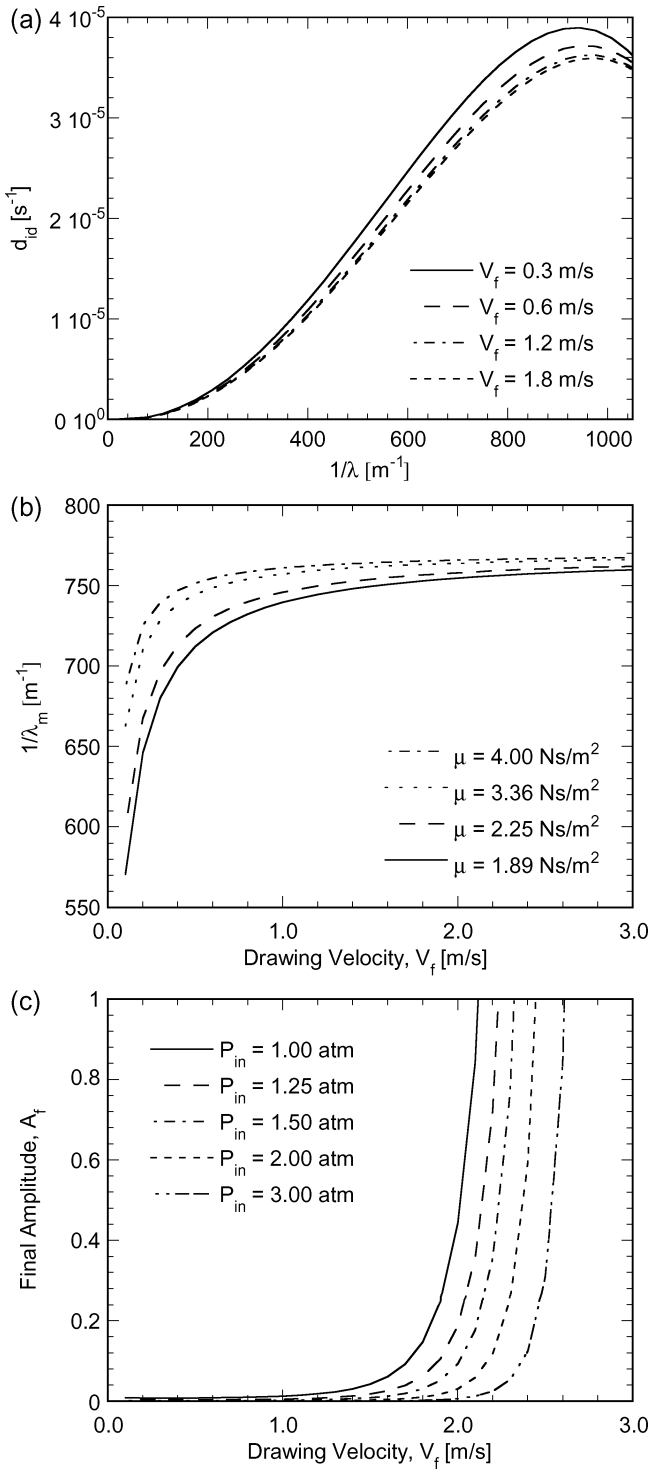

Fig. 12. (a) Dimensional amplitude growth rate d_{id} as a function the reciprocal of wave length $1/\lambda$ for different drawing velocity V_f. (b) Reciprocal of critical wave length $1/\lambda_m$ as a function of the drawing velocity V_f for different viscosity μ. (c) Final amplitude A_f as a function of the drawing velocity V_f for different inlet pressure p_{in}.

m/s. The relatively small d_{id} and physical time involved in Fig. 12(a) indicate that the final amplitude is not governed by the amplitude growth process, while large A_f mostly attributes to large value of A_i in Fig. 2.

Fig. 12(b) presents the reciprocal of the critical wave length $1/\lambda_m$ as a function of the drawing velocity V_f for four different values of viscosity μ; the other parameters assume the values in Fig. 12(a). It is observed that $1/\lambda_m$ increases monotonically with increasing V_f for fixed viscosity, and with increasing μ for fixed drawing velocity. Note that the critical wavenumber α_m in Fig. 7(a) decreases with increasing Re and S, owing to the decreased coating thickness h_0. The effects of the drawing velocity and the inlet pressure on the final amplitude are illustrated in Fig. 12(c), wherein the distance between the coater and the cure oven is taken to be 0.1 m, and the other parameters retain their values in Fig. 12(a). The trends in Fig. 12(c) follow those in Fig. 9(b), i.e., A_f increases monotonically with increasing V_f and decreasing p_{in}. For the case $P_{\text{in}} = 3.0$ atm, the coating thickness fluctuation reaches 100% of the nominal thickness when the drawing velocity $V_f > 2.6$ m/s, indicating strong instability of the coating flow under the processing conditions.

REFERENCES

[1] U. C. Paek, "Free drawing and polymer coating of silica glass optical fibers," *Trans. ASME*, vol. 121, pp. 774–788, 1999.

[2] U. C. Paek and C. M. Schroeder, "Optical performance of lightguide fibers coated at 10 m/s," in *Proc. Optical Fiber Communications Conf. (OFC 1985)*, San Diego, CA, 1985, p. 64.

[3] C. M. G. Jochem and J. W. C. Van Der Ligt, "Cooling and bubble-free coating of optical fibers at a high drawing rate," *J. Lightw. Technol.*, vol. LT-4, no. 7, pp. 739–742, Jul. 1986.

[4] C. Y. Zhao and S. H. K. Lee, "Physical considerations of a pressurized optical fiber coating process," *J. Materials Processing Manufacturing Sci.*, vol. 8, pp. 53–73, 1999.

[5] A. Panoliaskos, W. L. H. Ahallett, and I. Garis, "Prediction of optical fiber coating thickness," *Appl. Opt.*, vol. 24, pp. 2309–2312, 1985.

[6] S. Sakaguchi and T. Kimura, "High-speed drawing of optical fibers with pressurized coating," *J. Lightw. Technol.*, vol. LT-3, no. 3, pp. 669–673, Jun. 1985.

[7] H. Koaizawa, N. Orita, and T. Kamiya, "Study of coating diameter at high speed drawing," in *10th Int. Conf. Integrated Optics Optical Fiber Commun. Tech. Dig.*, vol. FA1-2, Hong Kong, 1995, pp. 4–5.

[8] M. Wagatsuma, T. Kimura, and S. Yamakawa, "Slip mechanism in optical fiber coating with open cup applicators," *J. Lightw. Technol.*, vol. LT-4, no. 4, pp. 1414–1419, Sep. 1986.

[9] K. Kobayashi, K. Tsurusaki, Y. Sato, and S. Araki, "High-speed coating of optical fibers with UV curable resins," in *Int. Wire Cable 40th Symp.*, 1991, pp. 126–133.

[10] S. Tomotika, "On the instability of a cylindrical thread of a viscous liquid surrounded by another viscous liquid," *Proc. Roy. Soc. A*, vol. 150, pp. 322–337, 1935.

[11] S. P. Lin and W. C. Liu, "Instability of film coating of wires and tubes," *AICHE J.*, vol. 21, pp. 775–782, 1975.

[12] S. L. Goren, "The instability of an annular thread of fluid," *J. Fluid Mech.*, vol. 12, pp. 309–319, 1962.

[13] J. Lin and C. Weng, "Linear stability analysis of condensate film flows down a vertical cylinder," *Chem. Eng. Comm.*, vol. 57, pp. 263–276, 1987.

[14] D. Quere, "Thin films flowing on vertical fibers," *Europhys. Lett.*, vol. 13, pp. 721–726, 1990.

[15] A. L. Frenkel, "Nonlinear theory of strongly undulating thin films flowing down vertical cylinders," *Europhys. Lett.*, vol. 18, pp. 583–588, 1992.

[16] P. Cheng, C. Chen, and H. Lai, "Nonlinear stability analysis of thin viscoelastic film flow traveling down along a vertical cylinder," *Nonlinear Dyn.*, vol. 24, pp. 305–332, 2001.

[17] N. Ashgriz and F. Mashayek, "Temporal analysis of capillary jet breakup," *J. Fluid Mech.*, vol. 291, pp. 163–190, 1995.

[18] X. Guan and R. Pitchumani, "Viscous fingering in a hele-shaw cell with finite viscosity ratio and interfacial tension," *ASME J. Fluid Engr.*, vol. 125, pp. 354–364, 2003.

[19] R. V. Birikh, V. A. Briskman, M. G. Velarde, and J. C. Legros, *Liquid Interfacial Systems Oscillations and Instability*. New York: Marcel Dekker, 2003.

Qibo Jiang received the M.S. degree in mechanical engineering from University of Connecticut, Storrs, in 2004. He is currently working toward the Ph.D. Degree at the University of Akron, OH.

His current research involves numerical and experimental investigation of injection molding process for the manufacturing of polymer composites

Fuzheng Yang received the B.S. and M.S. degrees in mechanical engineering from Tsinghua University, Beijing, China, in 1994 and 1997, respectively, and the Ph.D. degree in mechanical engineering from the University of Connecticut, Storrs, in 2002.

He is currently a Postdoctoral Fellow with the Advanced Materials and Technologies Laboratory, Department of Mechanical Engineering, University of Connecticut. His recent and current research activities are in the studies of advanced composite materials fabrication, fuel cells, MEMS, and optical fiber processing.

Ranga Pitchumani received the Ph.D. degree in mechanical engineering from Carnegie Mellon University, Pittsburgh, PA, in 1992

Heis the Distinguished Professor and Department Head of Mechanical Engineering at the University of Connecticut, Storrs. He was with the Center for Composite Materials, University of Delaware, prior to joining the University of Connecticut in 1995. His research interests are in the areas of advanced materials processing, micro and nanoscale phenomena, microdevices and microfabrication, and fuel cells. His research has been funded by NSF, ONR, AFOSR, ARO, NASA, Sandia National Laboratories, and Industries. He is the author of over 120 articles, seven edited book volumes, and five book chapters. He is an Associate Technical Editor for the ASME *Journal of Heat Transfer*, serves on the Editorial Board of the *Journal of Thermoplastic Composite Materials*, and has been a guest editor for *Polymer Composites*.

Dr. Pitchumani has received many awards including the Young Investigator Award from the Office of Naval Research and the Olin Faculty Award from OLIN Corporation. He is a Fellow of the ASME.